

A non-depolarizing CuTi neutron supermirror guide for PERC

A. Hollering^{a,b}, N. Rebrova^c, C. Klauser^d, Th. Lauer^{e,b,1}, B. Märkisch^{a,*}, U. Schmidt^c

^aPhysik-Department ENE, Technische Universität München, James-Frank-Str.1, D-85748 Garching, Germany

^bForschungsneutronenquelle Heinz Maier-Leibnitz, Lichtenbergstr. 1, D-85748 Garching, Germany

^cPhysikalisches Institut, Im Neuenheimer Feld 226, Universität Heidelberg, 69120 Heidelberg, Germany

^dInstitut Laue-Langevin, 71 avenue des Martyrs, F-38042 Grenoble, France

^eMovatec GmbH, Erfurter Straße 23, D-85386 Eching, Germany

Abstract

Neutron guides are used to transport slow neutrons from sources to experiments. Conventional neutron supermirror guides use alternating thin layers based on nickel and titanium. Due to the magnetic properties of nickel, their neutron reflection properties are spin-dependent, in particular when exposed to high magnetic fields. Motivated by the requirements of precision experiments on neutron beta decay, we present novel supermirrors based on copper and titanium, which preserve the neutron beam polarization. These show excellent reflectivity and prove to be very stable even when exposed to high temperatures.

Keywords: neutron supermirror, neutron guide, cold neutrons, magnetron sputtering

1. Introduction

Neutron guides are long glass channels whose inner surfaces are coated with a reflecting layer for angles of incidence up to a critical angle. They allow to transport cold and thermal neutrons away from a reactor or spallation source to experimental sites as far as 200 m away from the source [1, 2]. *Supermirrors*, first devised by Mezei and Dagleish [3], consist of a large number of thin double layers of typically Ni/Ti and varying in thickness such that the Bragg condition for neutrons with grazing incidence is fulfilled for a broad band of neutron de Broglie wavelengths. They hence increase the maximum angle of reflection at a given wavelength beyond the critical angle of total reflection of the best element Nickel by some factor m .

Within the neutron decay experiment PERC currently under construction at the MEPHISTO [4] beam line of the Heinz Maier-Leibnitz Zentrum (MLZ), Garching, Germany, an 8 m long guide inside an approximately 12 m long magnet system serves as decay volume [5, 6], with the guide surface largely in direction of the magnetic field. PERC will measure correlation coefficients in neutron β -decay in order to precisely determine the nucleon weak axial-coupling $g_A = \lambda g_V$, the first element of the quark-mixing Cabibbo-Kobayashi-Maskawa matrix V_{ud} and to search for physics beyond the Standard Model of particle

physics like novel scalar and tensor couplings. For a recent review of the field see [7].

In a guide, neutrons are reflected on the walls due to certain Bragg conditions that are defined by the layer thicknesses and material composition of a multilayer supermirror system. In the PERC experiment, the neutron spin of a highly polarized neutron beam has to be preserved on the level of 10^{-4} per bounce in order to match the precision requirements, see [5]. Supermirror coatings made of layers of ferromagnetic Ni and layers of paramagnetic Ti can depolarize the polarized neutron beam due to magnetic scattering if the magnetization has a component perpendicular to the scattering vector inside the coating [8]. Nickel with added molybdenum is commonly used for non-depolarising neutron guides [8, 9, 10]. Single layers of NiMo and NiP alloys are used for non-depolarizing guides for ultra-cold neutrons (UCNs), as well as a number of other materials, see [11, 12] and references therein.

In this paper, we present a novel neutron supermirror system made of Cu/Ti layers, the optimization procedure and its properties. A coating made of diamagnetic Cu and weakly paramagnetic Ti should be nearly non-magnetic even in strong magnetic fields of ≈ 2 T and can hence maintain the neutron polarization on the highest level.

In order to optimize the new supermirrors, we make use of different characterization techniques. We present the experimental results of various Cu/Ti single layers, multilayers of alternating bilayers of constant thickness, and neutron supermirrors produced by pulsed DC and RF magnetron sputtering. We studied the effects of pure nitrogen inside the Ti with X-ray reflection (XRR) and X-ray diffraction (XRD). The thermal stability was evaluated by neutron reflectivity measurements before and after heat

*Corresponding author

Email addresses: alexander.hollering@tum.de (A. Hollering), rebrova@jinr.ru (N. Rebrova), Christine.Klauser@psi.ch (C. Klauser), maerkisch@ph.tum.de (B. Märkisch), ulrich.schmidt@physi.uni-heidelberg.de (U. Schmidt)

¹Present address: MagTec GmbH, Bahnstraße 73, 67158 Ellerstadt

treatment. The model developed for the roughness growth inside a supermirror structure agrees well with the experimental data. The material composition of the layers was investigated using elastic recoil detection (ERD) [13] at the Q3D instrument [14] of the Maier-Leibnitz Laboratory (MLL), Garching. Depolarization measurements of early supermirrors were performed at the PF1b beam line [15] of the Institut Laue-Langevin (ILL), Grenoble, France, using an opaque test bench with polarized ^3He spin-filter cells [16, 17].

2. Experimental details

The substrate material has max. dimensions of $200 \times 300 \text{ mm}^2$ and the max. capacity of the sputtering machine is $300 \times 1200 \text{ mm}^2$. The Cu films were deposited by RF magnetron sputtering with a frequency of 13.56 MHz. The Ti films were deposited using pulsed DC magnetron sputtering with a frequency of 50 kHz and an additional substrate bias voltage. The base pressure of the system was 8×10^{-7} mbar and the pressures during sputtering were 5.4×10^{-3} mbar for Ti and 1.9×10^{-3} mbar for Cu. The sputtering power for both materials was set to 500 W. The distance between substrate and sputtering head was 150 mm. During the Ti sputter process, N_2 gas was admixed with the Ar sputter gas.

The samples consisting of TiN_x single layers (with x up to $\approx 30\%$) and Cu/ TiN_x multilayers and neutron supermirrors were deposited on float glass. Before coating, the glass mirrors were first cleaned in an ultra-sonic bath using alkaline mucasol cleaner and then processed further using isopropanol. In the sputtering chamber, they were cleaned in-situ using an Ar ion beam. The TiN_x single layers have thicknesses of 32 nm, 165 nm, and 300 nm. The multilayers consist of 40 bilayers of equal thickness of 6.6 nm for TiN_x and 6.9 nm for Cu. The neutron supermirrors consist of 95 bilayers Cu/ TiN_x with varying thickness.

The density, thickness and surface roughness of each film were determined by XRR measurements in $\Theta/2\Theta$ mode using $\text{CuK}\alpha$ radiation (1.54 Å) on a Bruker D8 diffractometer. The lattice parameters were determined by XRD measurements on the same device in $\Theta/2\Theta$ mode and in grazing incidence mode (GIXRD).

The neutron reflectivity (NR) curves of the multilayers and supermirrors were measured at the instrument TREFF at FRM II [18]. The NR investigations were performed at a fixed neutron wavelength of 4.8 Å in $\Theta/2\Theta$ mode. The resistance to heat treatment of the neutron supermirrors was also verified by NR at TREFF.

3. Results and discussion

3.1. Effects of impurities on single- and multilayers

A previous attempt at a Cu/Ti based supermirror with 20 bilayers is documented in Ref. [19]. The quality of the data did not allow conclusions on the effect of the high

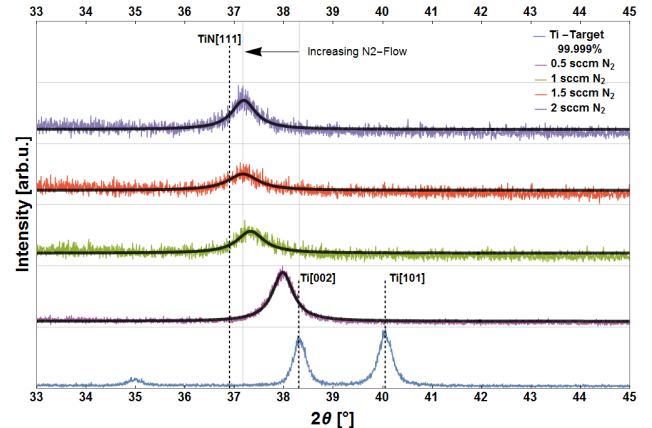


Figure 1: XRD on single layers of Ti and TiN_x with varying nitrogen flow during deposition. The black lines correspond to the fits of peak positions listed in Tab. 1.

nitrogen flow [sccm]	peak position [°]	peak width [°]
0	38.321(1)	0.136(1)
0.5	37.978(3)	0.251(5)
1	37.326(20)	0.33(3)
1.5	37.173(31)	0.38(4)
2	37.187(15)	0.30(2)

Table 1: Peak positions obtained by fitting the XRD data from TiN_x single layers shown in Fig. 1. The nitrogen flow during sputtering is given in *standard cubic centimeters per minute* (sccm).

mobility of Cu, which we find to be significant as shown below. The TiN_x layers can form an effective interdiffusion barrier [20, 21, 22, 23]. Using air as reactive sputtering gas as is commonly done for Ni layers [24] could lead to ferromagnetic clusters caused by copper oxides [25]. We consequently investigated the effects of a pure nitrogen admixture on the microstructure of the Ti layers by using XRD on samples with a nominal thickness of 300 nm deposited on float glass.

The addition of nitrogen to the Ar sputtering gas leads to a dilatation of the Ti lattice. The pure Ti target material shows two preferential planes, namely [002] and [101]. The Ti layer grown under pure Ar atmosphere shows the [002] plane, which gradually changes to the [111] plane of the TiN compound [26] with increasing nitrogen content. The [101] plane of pure Ti disappears. Generally, the reactively deposited Ti layers tend to grow more in amorphous structure. Fig. 1 shows the results of the XRD measurements on samples with different admixtures of N_2 .

We expect that the observed change in crystal structure and the nitrogen inside the Ti limit the interdiffusion for the multilayer structure and reduce roughness growth from layer to layer. As a downside, an increasing N_2 concentration also lowers the neutron optical contrast between the layers.

Fig. 2 shows three NR measurements of multilayers deposited with different nitrogen admixtures. As the mirrors each consist of 40 bilayers with equal layer thicknesses, we

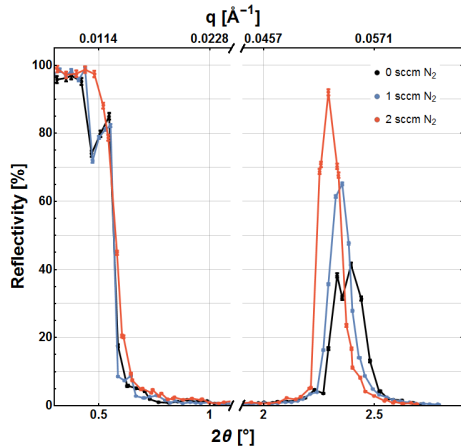


Figure 2: Neutron reflectivity curves of three multilayers with varying N_2 gas flow during sputtering. To help distinguish the peaks, data points are connected with colored lines. We observe total reflection from the top layer as well as a single Bragg peak from the multilayer with all bilayers of equal thickness. According to our modeling, the behavior at the edge can qualitatively be attributed to additional interference due to the inter-layer diffusion.

obtain constructive interference at a particular Bragg angle of reflection, as well as total reflection from the top layer below a critical angle.

The interpretation of such NR measurements is non-trivial. The roughness of the layers and interdiffusion of the different layer materials have very similar impact on the neutron reflectivity. It is hence not possible to distinguish between them from NR data. The high neutron reflectivity and the smallest peak width of the mirror sputtered with 2 sccm N_2 indicate that both, interlayer roughness and interdiffusion, are the lowest for this sample. With lower N_2 concentration, the peak width increases and the peak position shifts to larger angle of reflection. If the interface roughness increases, the proportion of diffuse scattered neutrons increases, which broadens the reflected peak. Assuming that two layers diffuse into one another, the effective thickness of the layers ‘seen’ by the incoming neutrons gets smaller. The thinner the layers are, the larger is the angle of Bragg reflection.

3.2. Single surface roughness

Based on the above results, we conclude that sputtering Ti reactively with 2 sccm N_2 would be the most promising option to obtain a Cu/ TiN_x neutron supermirror with highest possible reflectivity. We investigate the influence of a substrate bias voltage on the surface roughness of single TiN_x layers. Fig. 3 shows the roughness of six TiN_x single layers deposited on float glass with a thickness of 32 nm each, as calculated with our model, see section 3.5.

The surface roughness shows a clear dependency of the substrate bias voltage, which can be explained as follows: By applying a negative bias voltage to the substrate, some fraction of the ionized Ar atoms are accelerated onto the substrate surface. The surface roughness of the layer is the smallest between -115 V and -150 V, when the ions have

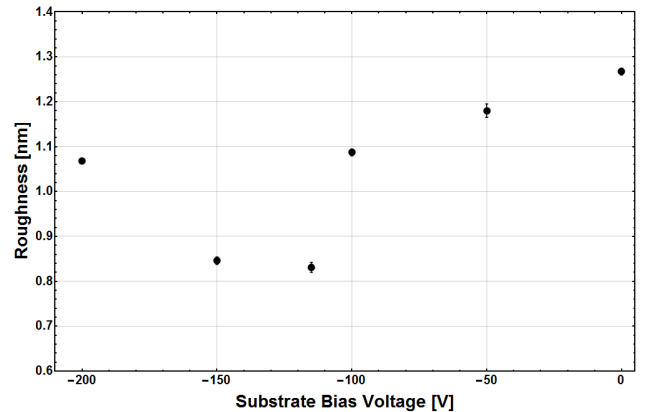


Figure 3: The surface roughness of TiN_x single layers for a N_2 gas flow of 2 sccm and with a thickness of 32 nm varies with the applied bias voltage and we observe a minimum at $\approx -115 \dots 150$ V. The roughness of the glass substrate is ≈ 0.6 nm.

enough energy to remove loosely bound atoms to smooth the surface. This can be interpreted as a nanopolishing procedure. For a bias voltage between -100 V and 0 V, the surface polishing effect decreases with the smaller energy of the Ar ions. For a voltage below -150 V, the ions have enough energy to kick out Ti atoms from the deposited layers. This effect is called re-sputtering and causes the layer roughness to increase [27].

The effect of applying a substrate bias voltage of -150 V is confirmed by the XRR measurement results shown in Fig. 4. A 165 nm thick TiN_x layer, deposited without bias voltage is compared to a 167 nm layer deposited with additional bias voltage of -150 V. For the sample deposited without bias voltage, the green curve in the figure, which is calculated according to our model, indicates a surface roughness of ≈ 6.5 nm. The difference between the green theoretical curve and the measurement is presumably coming from an ≈ 7 nm thick TiN_x interlayer formed by oxidation in the near surface region. For the sample sputtered with bias voltage, a surface roughness of $2.15(3)$ nm was determined (red curve). Taking the roughness of the float glass substrate of 0.6 nm into account, and assuming a linear growth of roughness with thickness, this corresponds to a roughness growth rate of only 0.09 \AA nm^{-1} .

3.3. Neutron supermirror

Taking into account our investigations on single- and multilayers, as well as improving the sputtering conditions, we produced Cu/ TiN_x neutron supermirrors with a high reflectivity of $> 90\%$ at the critical angle of reflection in the best case. For the sample shown in Fig. 5, this reflectivity is 92% .

The layer sequence for the mirrors was calculated by the following method: We approximate the layer sequence we obtain according to Ref. [3] for each material separately by a 5 point interpolation function. Then we calculate the reflectivity including our roughness growth model and optimize the reflectivity by varying the supporting points of

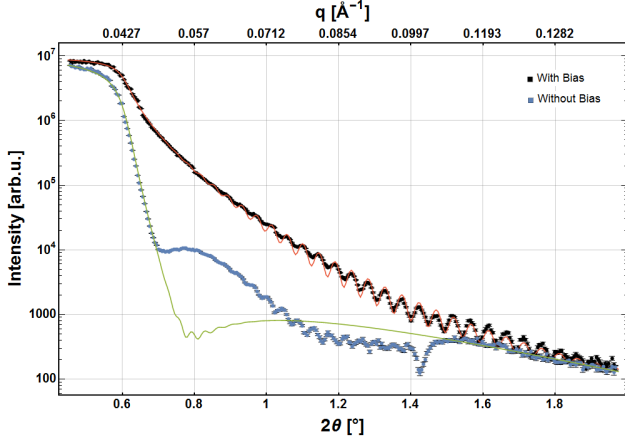


Figure 4: XRR measurement of 165 nm thick TiN_x layers deposited with a N_2 gas flow of 2 sccm and with or without substrate bias voltage. The red curve shows the fit result, with a surface roughness of only 2.15(3) nm. The green curve is not a fit, but a calculation assuming a roughness of ≈ 6.5 nm.

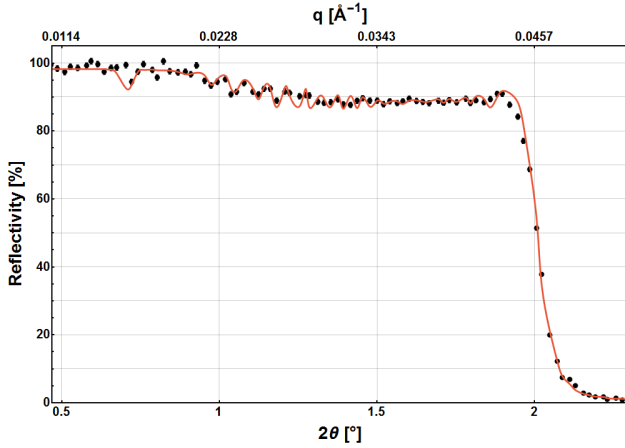


Figure 5: Neutron reflectivity measurement of a Cu/TiN_x $m = 2$ neutron supermirror with reflectivity of above 90%. The red curve is a fit using our roughness growth model in Eq. (1). The reduced χ^2 -value of the fit is 6.8.

the sequence interpolating function with a stochastic annealing method. High-purity sputter targets (Cu 99.995%, Ti 99.999%) were used for the supermirror coatings to be free of any critical impurity like e.g. iron. The reflectivity measurements in Fig. 5 and Fig. 6 were performed in single reflection mode. The critical angle of reflection corresponds to $m = 2$, i.e. double the critical angle of natural nickel.

3.4. Temperature stability

Stability of the mirrors at elevated temperatures is important for two reasons. First, it indicates that the interdiffusion is indeed reduced by the addition of N to the Ti layers. Additionally, the guide will be located in the ≈ 12 m long warm bore of the PERC magnet. To improve the vacuum conditions there, the bore can be backed at 100 °C, see Ref. [6]. But this procedure must not degrade the neutron guide.

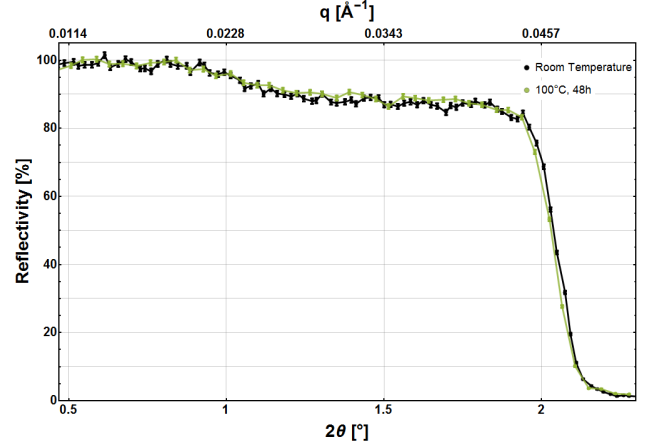


Figure 6: NR measurement of a Cu/TiN_x $m = 2$ supermirror consisting of 95 bilayers with a reflectivity of $R = 85\%$ before and after baking for 48 h at 100 °C. Measurement points are connected by lines to help distinguish the data sets.

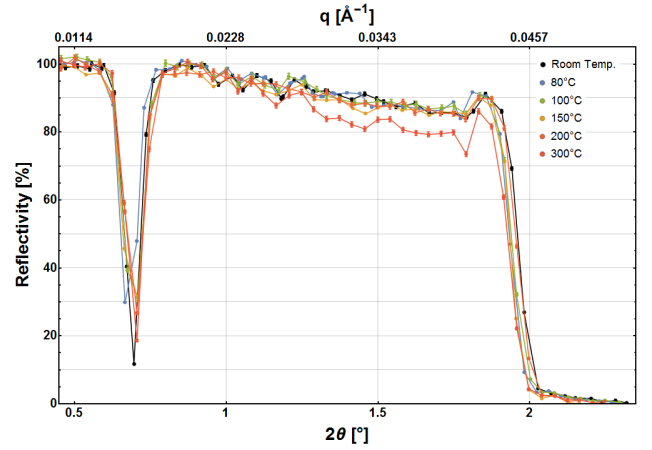


Figure 7: NR measurement of an early Cu/TiN_x $m = 1.95$ supermirror after subsequent baking for 12 h at 80 to 300 °C. Only after baking at 300 °C the reflectivity decreases significantly. The dip in reflectivity is due to a missing top-layer. Measurement points are connected by lines to help distinguish the data sets.

In Fig. 6 we present the NR measurement of one mirror with slightly lower reflectivity, which was used for thermal stability evaluation. The mirrors were deposited on standard float glass. The supermirror coating consists of 95 Cu/TiN_x bilayers with varying thickness. The mirror shows an excellent temperature stability. Still after baking for 48 h at a temperature of 100 °C, the neutron reflectivity remains practically unchanged.

Tests at higher temperatures were performed with an earlier sample. This was produced using low-purity targets and unfortunately suffered from a production error, a missing top-layer. The overall performance of this early sample is still worse than the recent result shown in Fig. 5. The sample was subsequently heated for 12 h at 80, 100, 150, 200 and 300 °C, and the neutron reflectivity was measured after each treatment. The results in Fig. 7 show that only baking at 300 °C has a significant

effect.

3.5. Roughness growth model

To describe the roughness growth inside the Cu/TiN_x supermirror stack, we need to account for the effect of interdiffusion. The new model was expanded and integrated into an existing fit routine used for the description of Ni/Ti supermirrors. The roughness of the *i*-th layer is given by the roughness of the substrate r_{sub} , a constant (effective) roughness due to interdiffusion r_{diff} and a term which describes the roughness accretion r with thickness:

$$r_i = r_{\text{sub}} + r_{\text{diff}} + r \cdot \left(\frac{d_i}{d_{\text{tot},i}} \right)^p, \quad (1)$$

where d_i and $d_{\text{tot},i}$ are the thicknesses of the *i*-th layer and all layers below, respectively, and p is the power of the roughness growth. We include roughness in our reflectivity calculation by folding the step function of the neutron optical potential at the layer borders with a Gaussian function where the standard deviation is given by the roughness except for r_{diff} . Here, the Gaussian function is replaced by a double-sided decaying exponential which leads to a better approximation of a diffusion profile.

r_{sub} [nm]	0.80(2)
r [nm]	2.41(9)
r_{diff} [nm]	0.79(2)
p	1.41(6)
red. χ^2 of the fit	6.8

Table 2: Roughness parameters from a fit to the reflectivity data of the Cu/TiN_x ($m = 2$, 190 layers) neutron supermirror shown in Fig. 5 as parametrized by Eq. (1).

For sputtering without ion plating, the deposited layer follows purely statistical roughness growth with $p = 0.5$, similar to snow flakes accumulating on smooth surfaces. For our Cu/TiN_x supermirrors produced with a bias voltage of -150 V we obtain $p > 1$, as the surface is polished in-situ by the incoming accelerated particles. The resulting roughness growth parameters for the red curve shown in Fig. 5 are listed in Tab. 2.

For a total thickness of the supermirror coating of ≈ 2 μm , the surface roughness ($r_{\text{sub}} + r_{\text{diff}} + r$) of the supermirror is only 4 nm. We observe the parameter $p > 1$, which indicates that the roughness growth is small in the beginning and increasing with the overall coating thickness. This effect can be explained by the small surface roughness of the substrate, which helps to keep the roughness low from the beginning and as well as by the fact, that the first layers have only a thickness of a few nanometers, where amorphous growth is favored and crystal growth suppressed. This roughness model might also prove helpful for the understanding of conventional supermirrors with higher m -values.

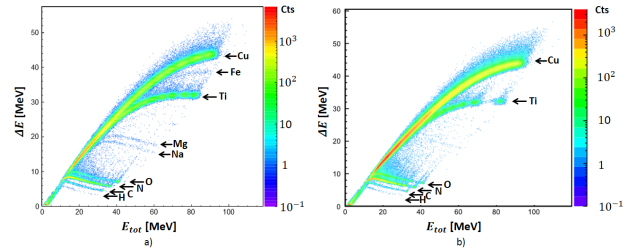


Figure 8: Element identification with ERD. **a)** A Cu/Ti supermirror created using targets with purities of 99.95 % for Cu and 99.6 % for Ti. Additional impurities like Na, Mg and Fe are detected.

b) Measurement of a Cu/Ti supermirror created using targets with purities of 99.995 % for Cu and 99.999 % for Ti. Here, no Fe is detectable.

3.6. Magnetic properties

The presence of magnetic roughness in layers, as is typical for ferromagnetic materials, causes depolarization of neutrons. We investigate early mirrors produced using a less pure Ti target (99.5%), which is known to contain traces of iron due to the production process. At the PF1b beamline of the ILL, we characterise these samples with m -values up to 1.2 with an in-plane magnetic field of up to 0.82 T using an opaque test bench with two ^3He neutron spin filter cells. The setup is described in Fig. 4 of Ref. [17], where it was used to characterize neutron polarizers. The measurement technique is sensitive to polarization and depolarization effects below the 10^{-4} level. With these early mirror samples, we find depolarization of $6(4) \times 10^{-5}$. More details on this experiment can be found in [28].

We note that Ref. [11] finds depolarisation at the level of a few times 10^{-5} per bounce for UCNs on single NiMo and Cu layers, but the application to our case with cold neutrons and high magnetic fields is not straight-forward.

Given the demanding (de)polarization criteria of the neutron decay measurement with PERC and its high magnetic field of 1.5 T, and the in total thicker layer sequence of the envisaged $m = 2$ supermirror, we switch to highly pure Ti targets for further development. The material composition of the layer sequence was investigated using elastic recoil detection (ERD) using an 170 MeV ^{127}I ion beam at the Q3D instrument at the MLL. The impurities Na, Mg and Fe, which were found in the Ti Target with 99.6 % purity, can be explained by the Kroll production process [29] and are consistent with the material's technical data sheet. In the Ti targets with 99.999 % purity, no Fe impurity was detectable, see Fig. 8. Such targets are typically produced by the Van-Arkel-de-Boer process [30]. Validation measurements with the opaque test bench using the new $m = 2$ mirrors are planned.

4. Conclusion

We demonstrate that the addition of N to the Ti layers results in an effective interdiffusion barrier for multilayer

structures of Cu/TiN_x. X-ray diffraction measurements indicate a dilatation of the Ti lattice and a reorientation of the Ti grains from preferential [002] to [111] with increasing nitrogen content. The addition of nitrogen also increases the long-term and temperature stability of the multilayers. X-ray reflectivity measurements show very smooth layer interfaces for layers produced with ion plating sputtering technology.

Neutron reflectivity investigations confirm, that $m = 2$ Cu/TiN_x non-depolarizing neutron supermirrors with a reflectivity above 90 % can be produced. Compared to Ni/Ti mirrors, the reflectivity at the maximum angle is lower by a few percent only. Background due to neutron absorption in PERC will hence be as low as envisaged in Ref. [5]. The excellent thermal stability will enable baking-out the neutron guide inside the warm bore of the PERC magnet [6] to obtain very good high vacuum conditions. Our new model for roughness growth of the supermirror layers enables an excellent description of the neutron reflectivity measurements.

Acknowledgment

This work is in part based upon experiments performed at the TREFF instrument operated by FRM II and at the X-ray diffractometer of the neutron optics group at the MLZ, and upon experiments at the PF1b instrument of the ILL, and the Q3D instrument at the MLL. The authors gratefully acknowledge the support by T. Soldner, ILL, with the depolarization measurements and thank A. Bergmaier for his support with the ERD measurements.

This work was supported by the Priority Program SPP 1491 of the German Research Foundation (DFG), contract No. LA2835/2-1, SCH2708/1-2, and SO1058/1-1.

References

- [1] S. Holm-Dahlin, M. A. Olsen, M. Bertelsen, J. O. Birk, K. Lefmann, Optimization of performance, price, and background of long neutron guides for European Spallation Source, *Quantum Beam Science* 3 (3) (2019). doi:10.3390/qubs3030016.
- [2] K. H. Andersen, et al., The instrument suite of the European Spallation Source, *Nuclear Instruments and Methods in Physics Research Section A: Accelerators, Spectrometers, Detectors and Associated Equipment* 957 (2020) 163402. doi:10.1016/j.nima.2020.163402.
- [3] F. Mezei, P.A. Dagleish, *Corrigendum and first experimental evidence on neutron supermirrors*, *Communications on Physics (London)* 45 (2) (1977) 41–43. URL <https://www.ill.eu/neutrons-for-society/neutron-technology/optics/the-founding-papers>
- [4] Heinz Maier-Leibnitz Zentrum, et al., MEPHISTO: Facility for particle physics with cold neutrons, *Journal of large-scale research facilities* 1 (A21) (2015). doi:10.17815/jlsrf-1-48.
- [5] D. Dubbers, H. Abele, S. Baeßler, B. Märkisch, M. Schumann, T. Soldner, O. Zimmer, A clean, bright, and versatile source of neutron decay products, *Nucl. Instrum. Methods Phys. Res., Sect. A* 596 (2) (2008) 238 – 247. doi:10.1016/j.nima.2008.07.157.
- [6] X. Wang, C. Drescher, et al., Design of the magnet system of the neutron decay facility PERC, *EPJ Web Conf.* 219 (2019) 04007. doi:10.1051/epjconf/201921904007.
- [7] D. Dubbers, B. Märkisch, Precise measurements of the decay of free neutrons, *Annual Review of Nuclear and Particle Science* 71 (1) (2021). doi:10.1146/annurev-nucl-102419-043156.
- [8] J. Padiyath, J. Stahn, P. Allenspach, M. Horisberger, P. Böni, Influence of Mo in the Ni sublayers on the magnetization of Ni/Ti neutron supermirrors, *Physica B: Condensed Matter* 350 (1, Supplement) (2004) E237–E240, *Proceedings of the Third European Conference on Neutron Scattering*. doi:10.1016/j.physb.2004.03.059.
- [9] A. Schebetov, A. Kovalev, B. Peskov, N. Pleshanov, V. Pusenkov, P. Schubert-Bischoff, G. Shmelev, Z. Soroko, V. Syromyatnikov, V. Ul'yanov, A. Zaitsev, Multi-channel neutron guides of PNPI: results of neutron and X-ray reflectometry tests, *Nuclear Instruments and Methods in Physics Research Section A: Accelerators, Spectrometers, Detectors and Associated Equipment* 432 (2) (1999) 214–226. doi:10.1016/S0168-9002(99)00480-5.
- [10] R. Kovács-Mezei, T. Krist, Z. Révay, Non-magnetic supermirrors produced at Mirrotron Ltd., *Nuclear Instruments and Methods in Physics Research Section A: Accelerators, Spectrometers, Detectors and Associated Equipment* 586 (1) (2008) 51–54, *Proceedings of the European Workshop on Neutron Optics*. doi:10.1016/j.nima.2007.11.034.
- [11] V. Bondar, S. Chesnevskaya, M. Daum, B. Franke, P. Geltenbort, L. Göttl, E. Gutschiedl, J. Karch, M. Kasprzak, G. Kessler, K. Kirch, H.-C. Koch, A. Kraft, T. Lauer, B. Lauss, E. Pierre, G. Pignol, D. Reggiani, P. Schmidt-Wellenburg, Y. Sobolev, T. Zechlau, G. Zsigmond, Losses and depolarization of ultracold neutrons on neutron guide and storage materials, *Phys. Rev. C* 96 (2017) 035205. doi:10.1103/PhysRevC.96.035205.
- [12] Z. Tang, E. Adamek, A. Brandt, N. Callahan, S. Clayton, S. Currie, T. Ito, M. Makela, Y. Masuda, C. Morris, R. Pattie, J. Ramsey, D. Salvat, A. Saunders, A. Young, Measurement of spin-flip probabilities for ultracold neutrons interacting with nickel phosphorus coated surfaces, *Nuclear Instruments and Methods in Physics Research Section A: Accelerators, Spectrometers, Detectors and Associated Equipment* 827 (2016) 32–38. doi:10.1016/j.nima.2016.04.098.
- [13] A. Bergmaier, G. Dollinger, C. Frey, Quantitative elastic recoil detection, *Nuclear Instruments and Methods in Physics Research Section B: Beam Interactions with Materials and Atoms* 99 (1) (1995) 488 – 490, *Application of Accelerators in Research and Industry '94*. doi:10.1016/0168-583X(94)00666-0.
- [14] G. Dollinger, A. Bergmaier, L. Goergens, P. Neumaier, W. Vandervorst, S. Jakschik, High resolution elastic recoil detection, *Nuclear Instruments and Methods in Physics Research Section B: Beam Interactions with Materials and Atoms* 219–220 (2004) 333 – 343, *Proceedings of the Sixteenth International Conference on Ion Beam Analysis*. doi:10.1016/j.nimb.2004.01.079.
- [15] H. Abele, D. Dubbers, H. Häse, M. Klein, A. Knöpfler, M. Kreuz, T. Lauer, B. Märkisch, D. Mund, V. Nesvizhevsky, A. Petoukhov, C. Schmidt, M. Schumann, T. Soldner, Characterization of a ballistic supermirror neutron guide, *Nuclear Instruments and Methods in Physics Research Section A: Accelerators, Spectrometers, Detectors and Associated Equipment* 562 (1) (2006) 407–417. doi:10.1016/j.nima.2006.03.020.
- [16] C. Klauser, *High precision neutron polarization for PERC*, Ph.D. thesis, Technische Universität Wien (2013). URL <https://resolver.obvsg.at/urn:nbn:at:at-ubtuw:1-65521>
- [17] C. Klauser, T. Bigault, P. Böni, P. Courtois, A. Devishvili, N. Rebrova, M. Schneider, T. Soldner, Depolarization in polarizing supermirrors, *Nuclear Instruments and Methods in Physics Research Section A: Accelerators, Spectrometers, Detectors and Associated Equipment* 840 (2016) 181–185. doi:10.1016/j.nima.2016.09.056.
- [18] Heinz Maier-Leibnitz Zentrum et al., TREFF: Reflectometer and instrument component test beamline at MLZ, *Journal of large-scale research facilities* 3 (A121) (2017). doi:10.17815/jlsrf-3-161.

- [19] N. Pleshanov, V. Pusenikov, A. Schebetov, B. Peskov, G. Shmelev, E. Siber, Z. Soroko, On the use of specular neutron reflection in the study of roughness and interdiffusion in thin-film structures, *Physica B: Condensed Matter* 198 (1) (1994) 27–32. doi:10.1016/0921-4526(94)90119-8.
- [20] S.-Q. Wang, I. Raaijmakers, B. J. Burrow, S. Suthar, S. Redkar, K.-B. Kim, Reactively sputtered TiN as a diffusion barrier between Cu and Si, *Journal of Applied Physics* 68 (10) (1990) 5176–5187. doi:10.1063/1.347059.
- [21] J. O. Olowolafe, C. J. Mogab, R. B. Gregory, M. Kottke, Interdiffusions in Cu/reactive-ion-sputtered TiN, Cu/chemical-vapor-deposited TiN, Cu/TaN, and TaN/Cu/TaN thin-film structures: Low temperature diffusion analyses, *Journal of Applied Physics* 72 (9) (1992) 4099–4103. doi:10.1063/1.352242.
- [22] M.Y. Kwak and D.H. Shin and T.W. Kang and K.N. Kim, Characteristics of TiN barrier layer against Cu diffusion, *Thin Solid Films* 339 (1) (1999) 290 – 293. doi:10.1016/S0040-6090(98)01074-8.
- [23] D.-J. Kim, Y.-B. Jung, M.-B. Lee, Y.-H. Lee, J.-H. Lee, J.-H. Lee, Applicability of ALE TiN films as Cu/Si diffusion barriers, *Thin Solid Films* 372 (1) (2000) 276 – 283. doi:10.1016/S0040-6090(00)01049-X.
- [24] M. Senthil Kumar, P. Böni, S. Tixier, D. Clemens, Stress minimisation in sputtered Ni/Ti supermirrors, *Physica B: Condensed Matter* 241-243 (1997) 95–97, Proceedings of the International Conference on Neutron Scattering. doi:10.1016/S0921-4526(97)00520-6.
- [25] L. Radjehi, A. Djelloul, M. Bououdina, R. Siab, W. Tebib, Structural and magnetic properties of copper oxide films deposited by DC magnetron reactive sputtering, *Applied Physics A* 124 (2018) 723. doi:10.1007/s00339-018-2141-0.
- [26] K. Khojier, H. Savaloni, E. Shokrai, Z. Dehghani, N. Z. Dehnavi, Influence of argon gas flow on mechanical and electrical properties of sputtered titanium nitride thin films, *J. Theor. Appl. Phys.* 7 (2013) 37. doi:10.1186/2251-7235-7-55.
- [27] S. Logothetidis, I. Alexandrou, S. Kokkou, Optimization of TiN thin film growth with in situ monitoring: the effect of bias voltage and nitrogen flow rate, *Surface and Coatings Technology* 80 (1) (1996) 66–71. doi:10.1016/0257-8972(95)02687-8.
- [28] N. Rebrova, Development of a non-depolarizing neutron guide for PERC, Ph.D. thesis, Ruperto-Carola University of Heidelberg, Germany (2014). doi:10.11588/heidok.00017029.
- [29] W. Kroll, Method for manufacturing titanium and alloys thereof, United States Patent US2205854A (1940).
- [30] A. E. van Arkel, J. H. de Boer, Darstellung von reinem Titanium-, Zirkonium-, Hafnium- und Thoriummetall, *Z. anorg. u. alg. Chem.* 148 (1925) 345 – 350. doi:10.1002/zaac.19251480133.